Long-lasting hybrid quantum information processing in a cavity-protection regime

A. Chiesa,[1] P. Santini,[1] D. Gerace,[2] and S. Carretta[1]
[1]*Dipartimento di Fisica e Scienze della Terra, Università di Parma, I-43124 Parma, Italy*
[2]*Dipartimento di Fisica, Università di Pavia, via Bassi 6, I-27100 Pavia, Italy*
(Received 25 June 2015; revised manuscript received 2 March 2016; published 28 March 2016)

Implementing complex sequences of gates is crucial for any quantum computing architecture to become practical. This requires long-lived qubits which can be manipulated many times without errors. Here we propose a scheme to process hybrid qubits consisting of spin ensembles coupled to superconducting resonators in a *cavity-protection* regime, which enhances their coherence time by orders of magnitude. We perform numerical experiments for the quantum simulation of the XY model and the quantum Fourier transform, by including all the main decoherence mechanisms and assuming system parameters that are guaranteed by present technology.

DOI: 10.1103/PhysRevB.93.094432

I. INTRODUCTION

Hybrid quantum devices constitute one of the most promising platforms to build quantum computing architectures, such as quantum simulators or solvers of specific quantum algorithms [1]. In particular, spin ensembles (SEs) coupled to superconducting qubits [2,3] and resonators [4–8] represent a concrete possibility for prospective quantum technologies: Photons may serve as quantum buses thanks to their high mobility [9,10], whereas spins are preferential candidates to build reliable quantum memories based on their long coherence time. A considerable step further in this direction was recently made by our proposed scheme for quantum information processing with hybrid spin-photon qubits replacing the superconducting units to encode information [11–13]. In such a novel setting a single manipulation tool (the tunability of resonators frequencies) is sufficient to implement a universal set of gates. However, inhomogeneous broadening (IB) of SEs remains the major challenge to overcome before any of these proposals can practically be realized. It was recently pointed out that a strong spin-cavity coupling can provide a protection mechanism for spin-based memories as long as the spin flip energy is close to the resonator frequency [14,15]. Such a mechanism was recently demonstrated experimentally under resonant conditions [16]. Nevertheless, while great attention has been focused on the storage of excitations in the SE, a proposal to implement single or sequences of gates with high fidelity by long-lived SEs is still lacking.

In the present paper, we address this unsolved issue by operating the hybrid spin-photon qubits in a cavity-protected regime, thus exploiting the spins not only for storing but also for processing quantum information for long times. We show that by combining a suitable spin-1 system with a proper time-dependent tuning of the resonators frequency, a universal set of gates can be implemented with coherence times no longer limited by IB. This paves the way to the actual scalability of this hybrid architecture. On the one hand, scalability is made possible by the inherent definition of the long-lived qubits, represented by coupled SE-resonator devices that can be repeated in an array. On the other hand, the mobility of photons and the use of spin-1 ensembles are crucial to perform two-qubit gates between physically distant qubits, without much more demanding SWAP gates. These resources make the class of problems that can be realistically addressed much larger. As test examples, we report full numerical experiments for the digital quantum simulation of the XY model on a pair of qubits and for the quantum Fourier transform on a chain of three qubits, which constitutes the fundamental building block of the Shor's factoring algorithm [17]. The robustness of the scheme is demonstrated by realistically including the main sources of decoherence in a master equation formalism and working with state-of-the-art parameters. Remarkably, the experimental realization of the present proposal only requires assembling elements that have already been separately demonstrated.

II. SETUP AND HYBRID QUBIT ENCODING

Each qubit is encoded in a coplanar superconducting waveguide resonator, containing at most one photon, strongly coupled to an ensemble of N effective $S = 1$ spins. For the sake of clarity, we first describe the system in the absence of inhomogeneous broadening. The resonator quantized electromagnetic field is described by the boson Hamiltonian $\hat{H}_{\rm ph} = \omega_c^{\mu}(t)\hat{a}_{\mu}^{\dagger}\hat{a}_{\mu}$, where μ labels the resonator of tunable frequency $\omega_c^{\mu}(t)$. Let $m = 0$ be the ground state of the single spins, separated from the $m = -1$ and $m = 1$ states by excitation frequencies ω_{-1} and ω_1. By applying the rotating-wave approximation, the SE-resonator coupling can be modeled as

$$\hat{\tilde{H}}_{\text{spin-ph}} = \sum_{m=-1,1}\sum_{j=1}^{N} g_m(\hat{a}_{\mu}\ |m_j\rangle_{\mu\,\mu}\langle 0_j| + \text{H.c}). \qquad (1)$$

Here j labels the individual spins within the ensemble. Then it is convenient to introduce the collective spin lowering operator $\hat{\beta}_{\mu,m} = \frac{1}{\sqrt{N}}\sum_{j=1}^{N}|0_j\rangle_{\mu\,\mu}\langle m_j|$ and its adjoint $\hat{\beta}_{\mu,m}^{\dagger}$. In the limit of small number of excitations, the Holstein-Primakoff approximation holds. Hence, $\hat{\beta}_{\mu,m}$ and $\hat{\beta}_{\mu,m}^{\dagger}$ are boson operators [5], obeying the commutation relation $[\hat{\beta}_{\mu,m},\hat{\beta}_{\mu,m}^{\dagger}] = 1$. Therefore, the collective spin excitations behave like independent harmonic oscillators, described as boson fields $\hat{H}_{\text{spin}} = \sum_m \omega_m\hat{\beta}_{\mu,m}^{\dagger}\hat{\beta}_{\mu,m}$. Within this framework, the SE-photon interaction takes the form:

$$\hat{H}_{\text{spin-ph}} = \sum_{m=-1,1} G_m\ (\hat{a}_{\mu}\ \hat{\beta}_{\mu,m}^{\dagger} + \hat{a}_{\mu}^{\dagger}\hat{\beta}_{\mu,m}), \qquad (2)$$

where the collective SE-photon interaction $G_m = \sqrt{N} g_m$ has been enhanced by $\sqrt{N}$, if compared to the single spin coupling strength.

We now suppose to initialize the system by preparing each spin in its ground state: $|\phi_0\rangle_\mu \equiv |0_1 ... 0_N\rangle_\mu$, with a single photon in the resonator. If the resonator frequency is tuned to match the spin gap ω_{-1}, the SE can absorb the photon and collectively evolve into the state $|\phi_1\rangle_\mu = \hat{\beta}^\dagger_{\mu,-1}|\phi_0\rangle_\mu$. Within the single-excitation subspace of the system formed by the cavity mode and the SE, we introduce the hybrid dual-rail encoding of the qubit μ: The logical state $|0\rangle_\mu$ ($|1\rangle_\mu$) corresponds to zero (one) photons and a single (zero) quantum in the $m = -1$ spin oscillator in cavity μ. A similar encoding was introduced in our previous works [11,12], but considering effective spin-1/2 ensembles. Here, the $m = 1$ oscillator represents an additional degree of freedom that is exploited to temporarily store the photonic component of the qubit when performing two-qubit gates between distant qubits [13].

The elementary unit of the scalable array is shown in Fig. 1(a): It consists of two *logical* resonators encoding two qubits, and an interposed *auxiliary* cavity containing a nonlinear three-level system such as a transmon, which is used for two-qubit gates. This is described by

$$\hat{H}_{\rm tr} = \Omega_{01}|\psi_{1,\mu}\rangle\langle\psi_{1,\mu}| + (\Omega_{12} + \Omega_{01})|\psi_{2,\mu}\rangle\langle\psi_{2,\mu}| + (g_{01}\hat{a}_\mu|\psi_{1,\mu}\rangle\langle\psi_{0,\mu}| + g_{12}\hat{a}_\mu|\psi_{2,\mu}\rangle\langle\psi_{1,\mu}| + \text{H.c.}). \quad (3)$$

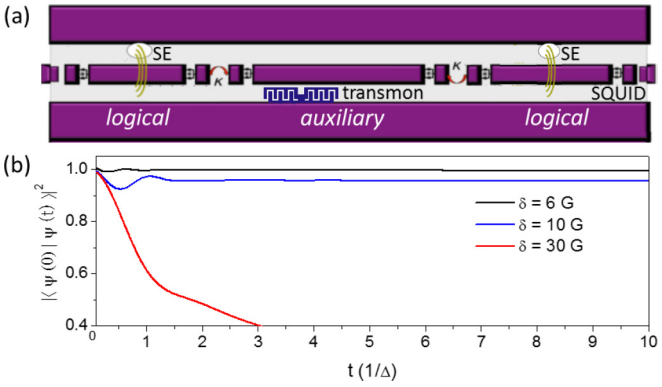

FIG. 1. (a) Elementary unit of the scalable setup. *Logical* resonators include an ensemble of $S = 1$ spins placed at the antinode of the magnetic field (rotational lines) of the cavity mode. The *auxiliary* resonator contains a transmon coupled to the electric field. The frequency of each resonator is tuned by means of a SQUID [21]. (b) Evolution of the super-radiant mode coupled to a bath of dark modes, calculated for different values of the spin-resonator detuning δ, while keeping the collective spin-resonator coupling G_{-1} to 30 MHz. We have assumed a Gaussian distribution for the spin gaps, with FWHM $\Delta = 1$ MHz. The system is initialized into an eigenstate of the single-qubit Hamiltonian, in order to point out the effect of the coupling with the dark modes. By decreasing δ, the system is more protected. $\delta = 6\,G_{-1}$ ensures that only 1% of the wave function is lost for long times.

Photon hopping is induced by capacitive coupling between neighboring resonators,

$$\hat{H}_{\text{ph-ph}} = -\kappa \sum_\mu (\hat{a}^\dagger_\mu \hat{a}_{\mu+1} + \text{H.c.}). \quad (4)$$

In the following, *logical* cavities will be labeled with odd μ, while *auxiliary* ones with even μ.

III. INHOMOGENEOUS BROADENING OF THE SPIN ENSEMBLE

A certain degree of spin inhomogeneity is unavoidable in real SEs and may result from slightly disordered spin environments or from random magnetic fields produced by surrounding nuclear magnetic moments. Among the N levels corresponding to one spin flip, a unique "super-radiant" collective spin-excitation couples to the resonator, while the other $N - 1$ "dark modes" are decoupled from the photon field. However, due to IB, the super-radiant excitation spontaneously decays into the quasicontinuum of dark modes within a timescale of order $\hbar/\Delta$, Δ being the width of the distribution of gaps in the SE. A possible way to deal with IB is to revert the associated Hamiltonian evolution by echo techniques [18–20], but implementing them within our encoding would be very demanding and would also require to tune the resonator quality factor in order to avoid emitting a microwave echo from the inverted spin ensemble.

Here we exploit only the tunability of individual resonator modes [8,21] to solve the problem and efficiently implement quantum gates. These are performed by keeping the SE in a "cavity-protection" regime [14–16]: A strong SE-resonator coupling induces an energy gap between the computational (super-radiant) and the noncomputational (dark) modes [14], thus effectively decoupling them. In the nonresonant regime, the energy shift of the super-radiant mode is of order G^2_{-1}/δ, where $\delta = \omega_{-1} - \omega_c(0)$ is the detuning between the bare resonator frequency and SE gap. By assuming a Gaussian broadening of width Δ, the cavity-protection condition is fulfilled if $2G^2_{-1}/\delta \gg \Delta$. However, reducing δ leads to unwanted oscillations of a significant fraction ($\sim G_{-1}/\delta$) of the wave function between logical states $|0\rangle_\mu$ and $|1\rangle_\mu$. Nevertheless, these oscillations can be compensated within our scheme, because they merely represent single-qubit rotations.

As a first step, we numerically determine the time evolution of the single-qubit wave-function $|\psi(t)\rangle_\mu$, coupled to a bath of dark modes, using the formalism of Ref. [15], outlined in Appendix A. To properly account for the effect of inhomogeneous broadening, we consider a distribution of the spin transition frequencies and of the spin-resonator couplings. Since we are interested in a very large number of spins N, we describe them by a continuous, Gaussian spectral density, spread around its central frequency ω^μ_c, with full width at half maximum (FWHM) Δ. The time evolution of the system wave function is then computed by the Laplace transform method, along the lines of Ref. [15].

Results are shown in Fig. 1(b) for a state initially prepared in $|\psi(0)\rangle_\mu = \cos\frac{\theta}{2}|0\rangle_\mu + \sin\frac{\theta}{2}|1\rangle_\mu$, which is an eigenstate of the single qubit Hamiltonian [Eq. (B1)] with $\cot\theta = \frac{\delta}{2G_{-1}}$. Thus, the observed evolution of $|\psi(t)\rangle_\mu$ is entirely due to the

coupling of the qubit with the dark modes. We have assumed a realistic coupling $G_{-1} = 30$ MHz and a SE with FWHM $\Delta = 1$ MHz [8,15]. Figure 1(b) clearly shows that the cavity-protection mechanism is enhanced on decreasing the detuning δ: For $\delta = 6\,G_{-1}$ only $\approx 1\%$ of the wave function is lost in the dark modes at long times. As expected, this is lower than the upper bound ($\Delta^2\delta^2/2\log 2G_{-1}^4 \approx 2.8\%$) obtained in Ref. [14]. Hence, in this regime the SE coherence time increases by orders of magnitudes and approaches the intrinsic single-spin time. The damping induced by IB can then be safely neglected. Similarly to what was done in the previous section with $\beta_{\mu,m}$ and $\beta^\dagger_{\mu,m}$, the spin excitations are described in the following by the boson operators $\hat{b}_{\mu,m} = \frac{1}{\bar{g}_m\sqrt{N}}\sum_{j=1}^{N} g_m^j |0_j\rangle_\mu\,{}_\mu\langle m_j|$ and $\hat{b}^\dagger_{\mu,m}$, where we have used $\bar{g}_m \equiv \sqrt{\sum_j |g_m^j|^2/N}$ to indicate the average single spin-photon coupling strength. The collective SE-photon interaction is then given by $\sqrt{N}\bar{g}_m$. The next task is to embed this cavity-protection mechanism within an efficient quantum computation scheme. This is by no means trivial, due to the unwanted oscillations of the wave function induced by the small detuning, which must be properly taken into account.

IV. QIP WITH AN INHOMOGENEOUSLY BROADENED SE

A. Choice of the spin system

The robustness of the scheme also relies on the choice of a suitable spin system. The ideal spin system has a narrow distribution of the energy gaps, which decays faster than a Lorentzian. Good candidates are spin systems with gaussian broadening, possibly isotropic and diluted in a nonmagnetic matrix, so as to avoid dipolar interactions, which typically lead to Lorentzian line shapes. Moreover, the spin gaps should be close to the frequency of current circuit QED resonators.

Hence, the best systems are the so-called S ions (like Fe^{3+} or Gd^{3+}) whose orbital angular momentum vanishes because of Hund's rules. This makes them practically insensitive to disorder in the environment. In addition, the number of nuclear spins should be minimized, as these produce random quasistatic magnetic fields causing IB. Linewidths as small as a fraction of Gauss are indeed observed in diluted magnetic semiconductors, such as Fe^{3+} in ZnS [22,23], whose nuclei are mostly spinless. Even narrower lines are observed for P-doped Si [24]. We note that the use of $S > 1$ spins increases G_{-1}, and thus the protection mechanism. The proper choice of the spin system leads to a degree of cavity protection much higher than that reported in the milestone experiment of Ref. [16], where the SE consisted of standard NV centers. This is not an ideal choice, since the spin-photon coupling is small ($\sim$8 MHz), and the gap distribution is broad ($\sim$9 MHz) and relatively fat-tailed.

To keep the experimental demonstration as easy as possible, we assume $\omega_c^\mu = 14$ GHz for the *logical*, and 10.2 GHz for the *auxiliary* resonators, lower than the frequencies employed in Ref. [6]. SEs fitting our scheme with a 14 GHz resonator can be easily found: Fe^{3+} impurities in the same Al_2O_3 matrix employed in Ref. [6] display suitable gaps with an applied magnetic field of $\sim$70 mT forming an angle of $\sim 70^\circ$ with the anisotropy axis (given an easy-plane anisotropy with $D = 5.15$ GHz [25]).

B. Elementary quantum gates

In the hybrid encoding, single-qubit rotations, $\hat{R}_x$ and $\hat{R}_y$, are obtained by temporarily bringing the frequency of the μth cavity, ω_c^μ, into resonance with the spin gap ω_{-1}, whereas $\hat{R}_z$ is obtained by a nonresonant variation of ω_c^μ (see Appendix C). As demonstrated by analytical calculations reported in Appendix B, the main consequence of working in a protected regime is the occurrence of unwanted one-qubit oscillations with frequency $\nu = \sqrt{G_{-1}^2 + \delta^2/4}$. These can be incorporated in the implementation of gates by choosing a starting time $\tilde{t}_s = 2n\pi/\nu$. However, gate starting times t_s cannot be chosen at will. For instance, the axis of one-qubit rotations in the x,y plane is selected by t_s [12]. The problem of matching the two constraints is solved by adding a"rephasing gate," consisting in significantly increasing δ (thus freezing unwanted oscillations) for a time $\Delta t_s = t_s - \tilde{t}_s$, with $\delta\,\Delta t_s = 4\pi n$. We stress that the time interval Δt_s is orders of magnitude shorter than that characterizing the damping due to IB. Hence, this temporary loss of cavity protection has no effects on the overall computation.

Two-qubit controlled-phase gates are implemented by sequentially moving the photonic component of *logical* resonators into the same *auxiliary* cavity, and inducing a two-step Rabi-flop involving the transmon (see Appendix C). The only part that is affected by the unwanted oscillations is the photon hopping between *logical* and *auxiliary* cavities, whose starting time needs to be chosen again as $t_s = 2n\pi/\nu$.

To test the performance of this scheme we first numerically determine the fidelity of a universal set of gates. In all the calculations reported below we also include decoherence effects. These are mainly due to photon loss and pure dephasing of the transmon [12], parameterized by the resonators quality factor (Q) and by the transmon dephasing time ($T_2^{\rm tr}$) in the Lindblad equation of motion:

$$\dot{\hat{\rho}} = -i[\hat{H},\hat{\rho}] + \sum_\mu \frac{\omega_c^\mu}{Q}\mathcal{L}_{\hat{a}_\mu}[\hat{\rho}] + \frac{1}{T_2^{\rm tr}}\sum_{\mu,i}\mathcal{L}_{|\psi_{i,\mu}\rangle\langle\psi_{i,\mu}|}[\hat{\rho}]. \quad (5)$$

Here $\mathcal{L}_{\hat{x}}[\hat{\rho}] = -\frac{1}{2}(\hat{x}^\dagger\hat{x}\hat{\rho} + \hat{\rho}\hat{x}^\dagger\hat{x}) + \hat{x}\hat{\rho}\hat{x}^\dagger$ and $\hat{H}$ is the full system Hamiltonian (see Appendix D). Additional sources of decoherence do not significantly affect the qubits dynamics, even on the timescale of several quantum gates (hundreds of ns, see numerical experiments reported below). Indeed, in the presently studied regime of parameters for the transmon $T_1^{\rm tr} > T_2^{\rm tr}$, typically in the range $T_1^{\rm tr}\sim$20–60 μs [27]. Furthermore, in single spins the pure dephasing time can reach the value of 0.1–1 ms [28], while the spin spontaneous emission time is completely negligible in most SEs at low temperatures (see, e.g., Ref. [28]). As far as photons are concerned, it has been experimentally shown that pure dephasing of the cavity modes is practically negligible (see, e.g., Ref. [29], where the measured value of the dephasing time approximately corresponds to twice the value of the photon decay time).

We list in Table I results obtained in the simulation of elementary quantum gates. It is worth noting that fidelities are very high, even with the inclusion of the most important decoherence channels and by operating in the cavity-protection regime. In the reported simulations, we assume the resonator frequency $\omega_c(0)/2\pi = 14$ GHz and the

TABLE I. Fidelity ($\mathcal{F}$) and duration of single- [$\hat{R}_x(\phi)$ and $\hat{R}_z(\phi)$] and two-qubit gates (controlled-NOT) [26], and to simulate the elementary terms of a generic two-body spin Hamiltonian (for $\lambda\tau = \pi/2$). Single-qubit rotations corresponds to simulating single-spin terms in the spin Hamiltonian (with $\phi = b\tau$). The fidelity has been computed on a random initial state, by assuming a Lindblad dynamics, with $Q = 10^6$ and $T_2^{\rm tr} = 10\mu s$, and operating in a cavity-protected regime with $\delta = 6\,G_{-1}$.

	$\hat{R}_x(\pi/2)$	$\hat{R}_z(\pi/2)$	$\hat{U}_{CNOT}$	$\hat{\mathcal{H}}^{(2)}_{yy}$	$\hat{\mathcal{H}}^{(2)}_{zz}$	$\hat{\mathcal{H}}^{(2)}_{yz}$
t	6.3 ns	0.5 ns	86.2 ns	86.2 ns	64.5 ns	86.2 ns
$\mathcal{F}$	99.77%	99.85%	98.75%	98.66%	99.02%	98.50%

photon hopping $\kappa = 30$ MHz. For the SE we use excitation frequencies $\omega_{-1}/2\pi = 14.18$ GHz, $\omega_1/2\pi = 12$ GHz and SE-photon couplings $G_{-1} = 30$ MHz, $G_{+1} = 33$ MHz. For the auxiliary resonator we assume a frequency $\omega_c(0)/2\pi = 10.2$ GHz, transmon gaps $\Omega_{01}/2\pi = 9.2$ GHz, $\Omega_{12}/2\pi = 8.3$ GHz and transmon-photon couplings $g_{01} = 30$ MHz, $g_{12} = 40$ MHz. At last, we use a detuning $\delta = 6\,G_{-1}$ for cavity protection. These parameters correspond to state-of-the-art technology [1,10].

V. NUMERICAL EXPERIMENTS

Here we report numerical experiments demonstrating the performance of our scheme in the implementation of some interesting quantum computation algorithms.

A. Digital simulation of the XY model

As a first example we consider a digital quantum simulator [30]. Digital techniques have been recently proposed in a superconducting circuitry architecture [13,31] and proof-of-principle demonstrations on a limited number of qubits have just been realized [32]. They are based on the decomposition [33] of the evolution operator of the target Hamiltonian $\hat{\mathcal{H}}$ into the product of terms acting on short time intervals τ. Since many problems can be mapped into a spin Hamiltonian, we focus on elementary terms consisting of one- ($\hat{\mathcal{H}}^{(1)}_\alpha$) and two-qubit ($\hat{\mathcal{H}}^{(2)}_{\alpha\beta}$) Hamiltonians, of the form: $\hat{\mathcal{H}}^{(1)}_\alpha = b\hat{s}_\alpha$ and $\hat{\mathcal{H}}^{(2)}_{\alpha\beta} = \lambda\hat{s}_{1\alpha}\hat{s}_{2\beta}$. The corresponding time evolution operator can be implemented by means of single- and two-qubit gates [34]. The fidelities calculated for the simulation of these elementary steps (Table I) are very high, thus demonstrating the effectiveness of our scheme. A proof-of-principle experiment that could be readily performed is the simulation of the dynamics resulting from an XY interaction ($\hat{\mathcal{H}}_{XY} = \lambda[\hat{s}_{1x}\hat{s}_{2x} + \hat{s}_{1y}\hat{s}_{2y}]$) between two spins $s = 1/2$, which is also the central step in the simulation of hopping processes in fermion Hamiltonians.

Figure 2(a) shows that the time evolution is very well reproduced (solid circles). These results can be compared with those obtained in a nonprotected regime (large spin-resonator detuning). The effect of IB is assessed by including in the master equation a damping term acting on the SE collective excitations $\gamma\sum_{\mu,m}\mathcal{L}_{\hat{b}_{\mu,m}}[\hat{\rho}]$, with $\gamma = \Delta/2\pi = 1$ MHz (empty circles), representing the irreversible leakage of the spin excitation in the dark modes [14,35]. It is evident

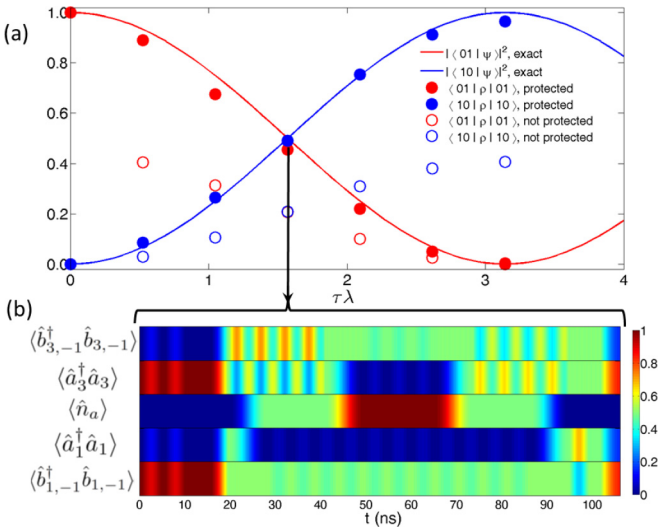

FIG. 2. (a) Simulation of the XY model with two hybrid qubits. Lines represent the exact evolution, whereas points are calculated with the Lindblad formalism ($Q = 10^6$, $T_2^{\rm tr} = 10\ \mu s$) within the cavity protection regime (solid circles) or not (empty). (b) Time dependence of the expectation values of number operators during the first half of the simulation of $\mathcal{H}_{XY}$ for the point $\tau\lambda = \pi/2$. The operator $\hat{n}_a = \hat{a}^\dagger_2\hat{a}_2 + |\psi_{1,2}\rangle\langle\psi_{1,2}| + 2|\psi_{2,2}\rangle\langle\psi_{2,2}|$ represents the total number of excitations in the *auxiliary* resonator.

from Fig. 2(a) that in the nonprotected regime IB would lead to completely unreliable results. We have also checked that a reduction of the transmon pure dephasing time from 10 to 1 μs does not significantly affect the simulation.

The expectation values of relevant operators in the computation of $\mathcal{H}_{xx}$ are reported as a color map in panel (b), where the oscillations of the boson occupations due to the cavity-protection regime can be clearly noticed. We finally stress that the scheme, besides defeating IB, enables the implementation of a large number of two-qubit gates in parallel.

B. Quantum Fourier transform

We now consider a chain of three qubits. An interesting proof-of-principle example is the implementation of the quantum Fourier transform (QFT), which constitutes the basic building block of powerful algorithms, such as Shor's and the quantum phase estimation algorithms [17]. The quantum circuit implementing QFT is shown in Fig. 3(a): It consists of three Hadamard and three controlled-phase gates. Figure 3(b) is a schematic view of the hardware at different times: *Logical* resonators are represented by squared, odd-numbered boxes, while *auxiliary* resonators are circular and even-numbered. The implementation of the QFT involves two-qubit gates between physically distant qubits: Here a controlled-$\hat{R}_z(\frac{\pi}{4})$ between qubits 1 and 5 is required [highlighted box in panel (a)]. It is important to note that to achieve this we do not need to fully transfer the state of qubit 1 into cavity 3 by means of a sequence of error-prone two-qubit gates, because the 1-3 SWAP is replaced by a much less demanding photon hopping process. Once the photon components of the two qubits involved in the controlled operation have been brought

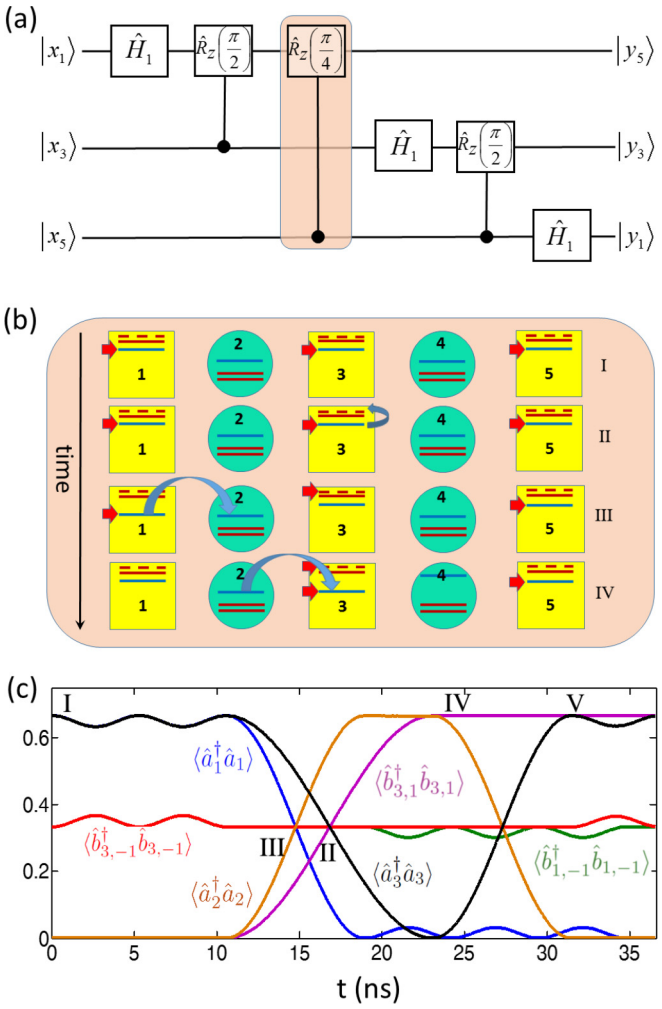

FIG. 3. (a) Quantum circuit implementing the QFT on three qubits. Each Hadamard gate can be decomposed into the product of two rotations: $\hat{H}_1 = i\hat{R}_y(\pi/2)\hat{R}_z(\pi)$. (b) Sketch of the three-qubit setup and of the elementary operations (numbered from I to IV) required to transfer a photon from *logical* resonator 1 to *logical* resonator 3. Here we show the $|1_1 1_3 1_5\rangle$ component of the wavefunction, with the excitations (red arrows) stored into the photonic degrees of freedom (blue lines). Red (continuous and dashed) lines represent the excitation energies of the spin oscillators ($m = -1$ and $m = 1$, respectively). (c) Expectation values of the photon ($\hat{a}_\mu$) and spin boson ($\hat{b}_{\mu,m}$) occupations in the photon-transfer process shown in (b), with the state initialized into $\frac{1}{\sqrt{3}}|0_1 0_3 0_5\rangle + \sqrt{\frac{2}{3}}|1_1 1_3 1_5\rangle$. Oscillations of $\hat{a}_5$ and $\hat{b}_{5,m}$ are not shown for clarity.

into neighboring *logical* resonators, the controlled-phase gate is implemented, and the photon components are finally brought back. We now illustrate this photon-transfer process, by reporting in Fig. 3(c) the time dependence of boson excitations, for a simple initial state $\frac{1}{\sqrt{3}}|0_1 0_3 0_5\rangle + \sqrt{\frac{2}{3}}|1_1 1_3 1_5\rangle$. In the idle phase (step I), each qubit is subject to oscillations between its photon and spin components, induced by the cavity-protected regime. After an integer number of oscillations, the photonic component of qubit 3 is absorbed into the $m = 1$ spin oscillator (II). Simultaneously, cavity 1 is brought into resonance with the neighboring *auxiliary* resonator 2, thus inducing a photon hopping (III). Then the same process is repeated with cavities 2 and 3, while detuning the *auxiliary* resonator 4 in order to avoid unwanted hoppings (IV). Finally qubits 1 and 5 are kept far from resonance for ∼ns to rephase their oscillations with those of the qubit 3 (V). We note that the photon component of qubit 3 is stored into the $m = 1$ spin oscillator only for the time required to the photonic component of qubit 1 to cross the resonator (∼15 *ns*). We have performed a numerical experiment by solving Eq. (5) for the whole QFT implementation for several random initial states. We find an average fidelity of about 93.6%, which is remarkably good since all the most important decoherence mechanisms have been taken into account. The total time required for the QFT on three qubits is about 300 ns.

VI. CONCLUSIONS

In conclusion, we have shown that a quantum computation scheme based on a hybrid spin-photon qubit encoding can solve the major issue of inhomogeneous broadening, by operating in a cavity-protected regime. We have corroborated this result by performing extensive numerical experiments on test examples, using parameters corresponding to state-of-the-art technology and concretely proposing spin systems suitable for an experimental implementation. The very high fidelity obtained in the simulation of paradigmatic algorithms, together with the enhanced coherence times of SEs opens the path to the scalability of the proposed architecture to a large array of resonators.

ACKNOWLEDGMENTS

We acknowledge very useful discussions with G. Amoretti, A. A. Houck, J. Raftery, and financial support from the Italian Ministry of Education and Research (MIUR) through Fondo Nazionale per la Ricerca di Base (FIRB), Project No. RBFR12RPD1.

APPENDIX A: TIME EVOLUTION OF THE INHOMOGENEOUSLY BROADENED SPIN ENSEMBLE

In this appendix, we study the dynamics of an inhomogeneously broadened ensemble of N spins coupled to a coplanar resonator. To this aim, we employ the formalism developed in Ref. [15]. For simplicity, we represent each spin as a two-level system, described by Pauli spin raising ($\hat{\sigma}_j^+ = |-1_j\rangle\langle 0_j|$) and lowering ($\hat{\sigma}_j^- = |0_j\rangle\langle -1_j|$) operators. The other degrees of freedom (e.g., the auxiliary spin level) are sufficiently detuned to produce no sizable effect on the system dynamics.

We introduce the vector $|\xi\rangle \equiv (\alpha_0, \alpha_1, \ldots, \alpha_N)$, whose components represent the probability amplitudes of the excitation in the resonator mode and in each spin, respectively: $\alpha_0 = \langle\emptyset|\hat{a}_\mu|\xi\rangle$, $\alpha_j = \langle\emptyset|\hat{\sigma}_j^-|\xi\rangle$. Here $|\emptyset\rangle$ is the state with no photons and the spins in $|\phi_0\rangle_\mu \equiv |0_1 \ldots 0_N\rangle_\mu$ and $j = 1, \ldots, N$. Using this notation, the logical states $|1\rangle_\mu \equiv \hat{a}_\mu^\dagger|\emptyset\rangle$ and $|0\rangle_\mu \equiv \hat{b}_{\mu,-1}^\dagger|\emptyset\rangle$ correspond to $(1,0,\ldots,0)$ and $(0, g_{-1}^1, \ldots, g_{-1}^N)/\bar{g}_{-1}\sqrt{N}$, respectively. The time evolution of

$|\xi\rangle$ can be modeled by the effective Hamiltonian [15]:

$$\hat{H}_{\rm eff} = \tilde{\omega}_c^{\mu}\hat{a}_{\mu}^{\dagger}\hat{a}_{\mu} + \sum_{j=1}^{N}\varepsilon_{-1}^{j}\frac{1-\hat{\sigma}_j^z}{2} + \sum_{j=1}^{N} g_{-1}^{j}(\hat{a}_{\mu}\hat{\sigma}_j^{+} + \hat{a}_{\mu}^{\dagger}\hat{\sigma}_j^{-}). \quad \text{(A1)}$$

Inhomogeneous broadening of the spin ensemble corresponds to a distribution of spin-resonator couplings, g_{-1}^{j}, and of transition frequencies, ε_{-1}^{j}, for the different spins. In the reported calculations, we have assumed a continuous, Gaussian distribution. $\tilde{\omega}_c^{\mu} = \omega_c^{\mu}(0) - i\Gamma/2$ is the complex photon frequency, with $\Gamma = \omega_c^{\mu}(0)/Q$ the photon loss rate and Q the quality factor of the resonator. $\hat{H}_{\rm eff}$ obeys a Schrödinger-like equation $\frac{d}{dt}|\xi(t)\rangle = -i\hat{H}_{\rm eff}|\xi(t)\rangle$. The time evolution of the qubit wave function is computed by the Laplace transform method, i.e.,

$$|\xi(t)\rangle = L^{-1}[(s + iH_{\rm eff})^{-1}|\xi(0)\rangle], \quad \text{(A2)}$$

where $L[f(t)] \equiv F(s) = \int_0^{\infty} e^{st} f(t)dt$. The choice of a continuous, Gaussian spectral density function for the spin frequencies allows one to obtain a closed expression for the scalar product $\langle\xi(t)|\xi(0)\rangle = \langle\xi(0)|e^{i\hat{H}_{\rm eff}t}|\xi(0)\rangle$. In particular, we report in the text the time evolution of a single-qubit wave function initialized in the state $\cos\frac{\theta}{2}|0\rangle_{\mu} + \sin\frac{\theta}{2}|1\rangle_{\mu}$, with $\cot\theta = \frac{\delta}{2G}$.

APPENDIX B: SEMIRESONANT EVOLUTION

Here we describe the evolution induced by the single-qubit Hamiltonian in a semiresonant regime, such that the spin-cavity detuning is comparable to the SE-cavity coupling strength. Contrary to what done in Appendix A, here we do not consider each individual spin transition, but we focus on the collective spin excitation (no matter its precise form) coupled to the resonator mode. The one-qubit Hamiltonian $\hat{H}_{1q}$, within the single excitation subspace, can be written as $\hat{H}_{1q} = G(|0\rangle\langle 1| + |1\rangle\langle 0|) + \delta|1\rangle\langle 1|$, i.e., in matrix form:

$$H_{1q} = \begin{pmatrix} 0 & G \\ G & \delta \end{pmatrix}, \quad \text{(B1)}$$

The eigenvectors of $\hat{H}_{1q}$ can be recast in the form $|\psi_-\rangle = \cos\frac{\theta}{2}|0\rangle - \sin\frac{\theta}{2}|1\rangle$ and $|\psi_+\rangle = \sin\frac{\theta}{2}|0\rangle + \cos\frac{\theta}{2}|1\rangle$, with $\theta = \operatorname{acot}\frac{\delta}{2G}$ and corresponding eigenvalues $E_{\pm} = \frac{\delta}{2} \pm \sqrt{G^2 + \delta^2/4}$. The unitary operator which describes the semiresonant evolution, in interaction picture is

$$U = e^{-i\frac{\delta\tau}{2}}\begin{pmatrix} \cos\nu\tau + \frac{i\delta}{\sqrt{\delta^2+4G^2}}\sin\nu\tau & -\frac{2iGe^{-i\delta t_0}}{\sqrt{\delta^2+4G^2}}\sin\nu\tau \\ -\frac{2iGe^{i\delta t_0}}{\sqrt{\delta^2+4G^2}}\sin\nu\tau & \cos\nu\tau - \frac{i\delta}{\sqrt{\delta^2+4G^2}}\sin\nu\tau \end{pmatrix}$$

where $\tau = t - t_0$, t_0 is the time at which U starts to act and we assumed Schrödinger and interaction picture coincident at $t = 0$. The oscillation frequency is $\nu = \sqrt{G^2 + \delta^2/4}$. Notice that this expression is valid only if the semiresonant evolution is followed by a phase gate $\hat{R}_z[-(\omega_c - \omega_{-1})\tau]$.

APPENDIX C: SINGLE- AND TWO-QUBIT GATES

1. Single-qubit rotations

One- and two-qubit gates are induced by "shift pulses," in which the frequency of cavity μ is varied by a quantity δ_c^{μ} for a suitable amount of time. In the idle state, the modes ω_c^{μ} and $\omega_c^{\mu+1}$ of neighboring cavities are far detuned and the effect of $\hat{H}_{\text{ph-ph}}$ is negligible. Single-qubit gates can thus be performed independently on each qubit, which can be individually addressed.

Off-resonance pulses are used to obtain a rotation about the z axis of the Bloch sphere. These induce a phase difference between the $|0\rangle$ and $|1\rangle$ states of the hybrid qubits, thus performing (a part from a global phase) the $\hat{R}_z$ gate:

$$R_z(-\delta_c^{\mu}T) = \begin{pmatrix} e^{i\delta_c^{\mu}T/2} & 0 \\ 0 & e^{-i\delta_c^{\mu}T/2} \end{pmatrix}. \quad \text{(C1)}$$

where we have assumed steplike pulses of amplitude δ_c^{μ} and duration T.

This coincides with a rotation around the z axis up to an overall phase, being $\hat{R}_z(\varphi) = e^{-i\hat{\sigma}_z\varphi/2} = e^{-i\varphi/2}\Phi(\varphi)$ and $\sigma_{\alpha=x,y,z}$ the Pauli matrices. Conversely, resonant pulses are employed to transfer the excitation between SEs and resonators. This produces (a part from a R_z rotation, see Ref. [12]) a generic rotation in the x-y plane of the Bloch sphere:

$$R_{xy}(\theta) = \begin{pmatrix} \cos(\theta/2) & -ie^{-i\delta_c^{\mu}t_0}\sin(\theta/2) \\ -ie^{i\delta_c^{\mu}t_0}\sin(\theta/2) & \cos(\theta/2) \end{pmatrix}, \quad \text{(C2)}$$

with $\theta = \bar{G}_{-1}T$. By properly tuning the initial time we can obtain rotations about x ($\delta_c^{\mu}t_0 = 2k\pi$) or y ($\delta_c^{\mu}t_0 = (4k+1)\pi/2$) axis, while the pulse duration controls the rotation angle. See Ref. [12] for a detailed derivation.

2. Controlled-phase gate

The Controlled-phase (Cφ) two-qubit gate is represented by the matrix:

$$U_{C\varphi} = \begin{pmatrix} 1 & 0 & 0 & 0 \\ 0 & 1 & 0 & 0 \\ 0 & 0 & 1 & 0 \\ 0 & 0 & 0 & e^{-i\varphi} \end{pmatrix}. \quad \text{(C3)}$$

It can be implemented by means of two-step semiresonant Rabi oscillations of the transmon state between $|\psi_{0,\mu+1}\rangle$ and $|\psi_{2,\mu+1}\rangle$. We describe here the Cφ multistep pulse sequence on two qubits initialized in the state $|1_{\mu}1_{\mu+2}\rangle$:

(1) The first step corresponds to the hopping of the photon from *logical* cavity μ to the *auxiliary* resonator $\mu + 1$

(interposed between qubits μ and $\mu+2$), by means of a π pulse that brings the two cavities into resonance.

(2) As a second step, the frequency of resonator $\mu+1$ ($\omega_c^{\mu+1}$) is tuned to Ω_{01} by means of a π pulse, which induces the transition to the intermediate state $|\psi_{1,\mu+1}\rangle$ of the transmon.

(3) A π pulse is exploited to induce the hopping of a second photon from *logical* cavity $\mu+2$ to the *auxiliary* resonator.

(4) Then a pulse of duration $\Delta t = \frac{\pi}{\sqrt{g_{12}^2+\delta_{12}^2/4}}$, where $\delta_{12} = \Omega_{12} - \omega_c^{\mu+1}$ is the detuning between the resonator mode and the $|\psi_{1,\mu+1}\rangle \rightarrow |\psi_{2,\mu+1}\rangle$ transition of the transmon, adds a phase $\varphi = \pi - \pi\frac{\delta_{12}}{\sqrt{\delta_{12}^2+4g_{12}^2}}$ to the system wave function [36].

(5) Finally, the repetition of the first three steps brings the state back to $|1_\mu 1_{\mu+2}\rangle$, with an overall phase φ. By properly setting the delay between the two π pulses corresponding to the previous steps (or by performing single-qubit phase shifts), the associated hopping processes yield a zero additional phase.

Conversely, the other basis states do not acquire any phase, due to the absence of at least one of the two photons (see Ref. [12]). Hence, the above sequence implements the Cφ gate. The use of an ensemble of effective $S=1$ spins ensures the possibility of implementing Controlled-phase gates between distant qubits (labeled A and B below), with no need of performing highly demanding and error-prone sequences of two-qubit SWAP gates. This is done by absorbing the photon component of each qubit μ interposed between A and B into the corresponding $m=1$ spin oscillator, while the photon components of A and B cross the resonator μ in moving into the same *auxiliary* resonator. This temporary storage is essential to avoid the simultaneous presence of two photons within the same resonator, which could corrupt the state of the qubit.

We finally stress that long-range two-qubit interactions are a key resource for the digital simulation of many interesting physical Hamiltonians, such as those involving interacting fermions in two or higher spatial dimensions, and for important algorithms, such as the quantum Fourier transform, which are often intractable for classical computers. We note that a large number of these long-range two-qubit gates can be implemented in parallel in the actual setup.

APPENDIX D: DENSITY MATRIX MASTER EQUATION

The time evolution of the system density matrix $\hat{\rho}$ is described within a Markovian approximation and a Lindblad-type dynamics, with the Liouville-von Neumann equation of motion [37]:

$$\frac{d}{dt}\hat{\rho} = -i[\hat{H},\hat{\rho}] + \sum_\mu \Gamma_\mu \mathcal{L}_{\hat{x}_\mu}[\hat{\rho}] + \sum_i \gamma_\mu \mathcal{L}_{\hat{x}_\mu^\dagger \hat{x}_\mu}[\hat{\rho}], \quad \text{(D1)}$$

being Γ_μ and γ_μ, respectively, the damping and pure-dephasing rates of the field $\hat{x}_\mu$. The Lindblad term for an arbitrary operator $\hat{x}$ is given by

$$\mathcal{L}_{\hat{x}}[\hat{\rho}] = -\tfrac{1}{2}(\hat{x}^\dagger\hat{x}\hat{\rho} + \hat{\rho}\hat{x}^\dagger\hat{x}) + \hat{x}\hat{\rho}\hat{x}^\dagger. \quad \text{(D2)}$$

The density matrix approach followed in the present paper allows us to include the effects of relaxation and pure dephasing on each element involved in the scheme. If the operator $\hat{x}_\mu$ destroys an excitation in the system, terms like $\mathcal{L}_{\hat{x}_\mu}[\hat{\rho}]$ account for energy losses, while pure dephasing processes are described by $\mathcal{L}_{\hat{x}_\mu^\dagger\hat{x}_\mu}[\hat{\rho}]$. For instance, the Lindblad term accounting for photon loss into resonator μ takes the form $\mathcal{L}_{\hat{a}_\mu}[\hat{\rho}] = -\frac{1}{2}(\hat{a}_\mu^\dagger\hat{a}_\mu\hat{\rho} + \hat{\rho}\hat{a}_\mu^\dagger\hat{a}_\mu) + \hat{a}_\mu\hat{\rho}\hat{a}_\mu^\dagger$, while pure dephasing of the transmon μ is expressed by $\sum_{i=1,2}|\psi_{i,\mu}\rangle\langle\psi_{i,\mu}|\hat{\rho}|\psi_{i,\mu}\rangle\langle\psi_{i,\mu}| - \frac{1}{2}(|\psi_{i,\mu}\rangle\langle\psi_{i,\mu}|\hat{\rho} + \hat{\rho}|\psi_{i,\mu}\rangle\langle\psi_{i,\mu}|)$. These are the most important contributions to decoherence, as shown in previous works [12]. We represent each field as a matrix in the Fock-states basis, and truncate it at a number of total excitations previously checked for convergence. The total Hamiltonian and the density matrix master equation of the whole system are built by tensor products of these operators. Then, the equation of motion for $\hat{\rho}$ is numerically integrated, in the interaction picture, by using a standard Runge-Kutta approximation.

[1] Z.-L. Xiang, S. Ashhab, J. Q. You, and F. Nori, Rev. Mod. Phys. **85**, 623 (2013).

[2] J. Koch, T. M. Yu, J. Gambetta, A. A. Houck, D. I. Schuster, J. Majer, A. Blais, M. H. Devoret, S. M. Girvin, and R. J. Schoelkopf, Phys. Rev. A **76**, 042319 (2007).

[3] R. Barends, J. Kelly, A. Megrant, A. Veitia, D. Sank, E. Jeffrey, T. C. White, J. Mutus, A. G. Fowler, B. Campbell, Y. Chen, Z. Chen, B. Chiaro, A. Dunsworth, C. Neill, P. O'Malley, P. Roushan, A. Vainsencher, J. Wenner, A. N. Korotkov, A. N. Cleland, and J. M. Martinis, Nature (London) **508**, 500 (2014).

[4] A. Imamoglu, Phys. Rev. Lett. **102**, 083602 (2009).

[5] J. H. Wesenberg, A. Ardavan, G. A. D. Briggs, J. J. L. Morton, R. J. Schoelkopf, D. I. Schuster, and K. Mølmer, Phys. Rev. Lett. **103**, 070502 (2009).

[6] D. I. Schuster, A. P. Sears, E. Ginossar, L. DiCarlo, L. Frunzio, J. J. L. Morton, H. Wu, G. A. D. Briggs, B. B. Buckley, D. D. Awschalom, and R. J. Schoelkopf, Phys. Rev. Lett. **105**, 140501 (2010).

[7] Y. Kubo, C. Grezes, A. Dewes, T. Umeda, J. Isoya, H. Sumiya, N. Morishita, H. Abe, S. Onoda, T. Ohshima, V. Jacques, A. Dréau, J.-F. Roch, I. Diniz, A. Auffèves, D. Vion, D. Esteve, and P. Bertet, Phys. Rev. Lett. **107**, 220501 (2011).

[8] Y. Kubo, I. Diniz, A. Dewes, V. Jacques, A. Dréau, J.-F. Roch, A. Auffèves, D. Vion, D. Esteve, and P. Bertet, Phys. Rev. A **85**, 012333 (2012).

[9] J. Majer, J. M. Chow, J. M. Gambetta, J. Koch, B. R. Johnson, J. A. Schreier, L. Frunzio, D. I. Schuster, A. A. Houck, A. Wallraff, A. Blais, M. H. Devoret, S. M. Girvin, and R. J. Schoelkopf, Nature (London) **449**, 443 (2007).

[10] S. Schmidt and J. Koch, Ann. Phys. **525**, 395 (2013).

[11] S. Carretta, A. Chiesa, F. Troiani, D. Gerace, G. Amoretti, and P. Santini, Phys. Rev. Lett. **111**, 110501 (2013).

[12] A. Chiesa, D. Gerace, F. Troiani, G. Amoretti, P. Santini, and S. Carretta, Phys. Rev. A **89**, 052308 (2014).

[13] A. Chiesa, P. Santini, D. Gerace, J. Raftery, A. A. Houck, and S. Carretta, Sci. Rep. **5**, 16036 (2015).

[14] Z. Kurucz, J. H. Wesenberg and K. Mølmer, Phys. Rev. A **83**, 053852 (2011).
[15] I. Diniz, S. Portolan, R. Ferreira, J.-M. Gérard, P. Bertet, and A. Auffèves, Phys. Rev. A **84**, 063810 (2011).
[16] S. Putz, D. O. Krimer, R. Amsüss, A. Valookaran, T. Nöbauer, J. Schmiedmayer, S. Rotter, and J. Majer, Nat. Phys. **10**, 720 (2014).
[17] M. A. Nielsen and I. L. Chuang, *Quantum Computation and Quantum Information* (Cambridge University Press, Cambridge, U. K., 2000).
[18] H. Wu, R. E. George, J. H. Wesenberg, K. Mølmer, D. I. Schuster, R. J. Schoelkopf, K. M. Itoh, A. Ardavan, J. J. L. Morton, and G. A. D. Briggs, Phys. Rev. Lett. **105**, 140503 (2010).
[19] B. Julsgaard, C. Grezes, P. Bertet and K. Mølmer, Phys. Rev. Lett. **110**, 250503 (2013).
[20] C. Grezes, B. Julsgaard, Y. Kubo, M. Stern, T. Umeda, J. Isoya, H. Sumiya, H. Abe, S. Onoda, T. Ohshima, V. Jacques, J. Esteve, D. Vion, D. Esteve, K. Mølmer, and P. Bertet, Phys. Rev. X **4**, 021049 (2014).
[21] A. Palacios-Laloy, F. Nguyen, F. Mallet, P. Bertet, D. Vion, and D. Esteve, J. Low Temp. Phys. **151**, 1034 (2008).
[22] W. C. Holton, J. Schneider, and T. L. Estle, Phys. Rev. **133**, A1638 (1964); A. Räuber and J. Schneider, Z. Naturforsch. **17a**, 266 (1962).
[23] E. R. Feher, Phys. Rev. **136**, A145 (1964).
[24] A. M. Tyryshkin, S. A. Lyon, A. V. Astashkin, and A. M. Raitsimring, Phys. Rev. B **68**, 193207 (2003).
[25] W. G. Farr, D. L. Creedon, M. Goryachev, K. Benmessai, and M. E. Tobar, Phys. Rev. B **88**, 224426 (2013).
[26] The unitary operator which implements a controlled-NOT gate ($\hat{U}_{CNOT}$) is obtained by combining a controlled-Z with two R_y rotations on the target qubit, i.e., $\hat{U}_{CNOT} = [\hat{I} \otimes \hat{R}_y(\frac{\pi}{2})]\hat{U}_{CZ}[\hat{I} \otimes \hat{R}_y(-\frac{\pi}{2})]$.
[27] H. Paik, D. I. Schuster, Lev S. Bishop, G. Kirchmair, G. Catelani, A. P. Sears, B. R. Johnson, M. J. Reagor, L. Frunzio, L. I. Glazman, S. M. Girvin, M. H. Devoret, and R. J. Schoelkopf, Phys. Rev. Lett. **107**, 240501 (2011).
[28] R. E. George, J. P. Edwards, and A. Ardavan, Phys. Rev. Lett. **110**, 027601 (2013).
[29] H. Wang, M. Hofheinz, M. Ansmann, R. C. Bialczak, E. Lucero, M. Neeley, A. D. O'Connell, D. Sank, J. Wenner, A. N. Cleland, and J. M. Martinis, Phys. Rev. Lett. **101**, 240401 (2008).
[30] I. M. Georgescu, S. Ashhab, and F. Nori, Rev. Mod. Phys. **86**, 153 (2014).
[31] U. L. Heras, A. Mezzacapo, L. Lamata, S. Filipp, A. Wallraff, and E. Solano, Phys. Rev. Lett. **112**, 200501 (2014).
[32] Y. Salathé, M. Mondal, M. Oppliger, J. Heinsoo, P. Kurpiers, A. Potočnik, A. Mezzacapo, U. Las Heras, L. Lamata, E. Solano, S. Filipp, and A. Wallraff, Phys. Rev. X **5**, 021027 (2015); R. Barends, L. Lamata, and J. Kelly, L. García-Álvarez, A. G. Fowler, A. Megrant, E. Jeffrey, T. C. White, D. Sank, J. Y. Mutus, B. Campbell, Yu Chen, Z. Chen, B. Chiaro, A. Dunsworth, I.-C. Hoi, C. Neill, P. J. J. O'Malley, C. Quintana, P. Roushan, A. Vainsencher, J. Wenner, E. Solano, and J. M. Martinis, Nat. Commun. **6**, 7654 (2015).
[33] S. Lloyd, Science **273**, 1073 (1996).
[34] P. Santini, S. Carretta, F. Troiani, and G. Amoretti, Phys. Rev. Lett. **107**, 230502 (2011).
[35] Y. Liu, J. You, and Q. Hou, Sci. Rep. **6**, 21775 (2016).
[36] M. Mariantoni, H. Wang, T. Yamamoto, M. Neeley, R. C. Bialczak, Y. Chen, M. Lenander, E. Lucero, A. D. O'Connell, D. Sank, M. Weides, J. Wenner, Y. Yin, J. Zhao, A. N. Korotkov, A. N. Cleland, and J. M. Martinis, Science **334**, 61 (2011).
[37] M. O. Scully and M. S. Zubairy, *Quantum Optics* (Cambridge University Press, Cambridge, UK, 1997).